Journal of Astronomical Telescopes, Instruments, and Systems

AstronomicalTelescopes.SPIEDigitalLibrary.org

Postirradiation behavior of p-channel charge-coupled devices irradiated at 153 K

Jason P. D. Gow
Daniel Wood
Neil J. Murray
David Burt
David J. Hall
Ben Dryer
Andrew D. Holland

SPIE.

Jason P. D. Gow, Daniel Wood, Neil J. Murray, David Burt, David J. Hall, Ben Dryer, Andrew D. Holland, "Postirradiation behavior of p-channel charge-coupled devices irradiated at 153 K," *J. Astron. Telesc. Instrum. Syst.* **2**(2), 026001 (2016), doi: 10.1117/1.JATIS.2.2.026001.

Postirradiation behavior of p-channel charge-coupled devices irradiated at 153 K

Jason P. D. Gow,[a,*] Daniel Wood,[a] Neil J. Murray,[a] David Burt,[b] David J. Hall,[a] Ben Dryer,[a] and Andrew D. Holland[a]
[a]The Open University, Centre for Electronic Imaging, Department of Physical Sciences, Milton Keynes MK7 6AA, United Kingdom
[b]e2v Technologies PLC, 106 Waterhouse Lane, Chelmsford, Essex CM1 2QU, United Kingdom

Abstract. The displacement damage hardness that can be achieved using p-channel charge-coupled devices (CCD) was originally demonstrated in 1997, and since then a number of other studies have demonstrated an improved tolerance to radiation-induced charge transfer inefficiency when compared to n-channel CCDs. A number of recent studies have also shown that the temperature history of the device after the irradiation impacts the performance of the detector, linked to the mobility of defects at different temperatures. The initial results from an e2v technologies p-channel CCD204 irradiated at 153 K with 10-MeV equivalent proton fluences of 1.24×10^9 and 1.24×10^{11} protons cm^{-2} is described. The dark current, cosmetic quality, and the number of defects identified using trap pumping immediately were monitored after the irradiation for a period of 150 h with the device held at 153 K and then after different periods of time at room temperature. The device also exhibited a flatband voltage shift of around 30 mV/krad, determined by the reduction in full well capacity. [DOI: 10.1117/1.JATIS.2.2.026001]

Keywords: charge-coupled devices; p-channel; cryogenic irradiation; proton radiation damage.

Paper 15080P received Nov. 16, 2015; accepted for publication May 13, 2016; published online Jun. 9, 2016.

1 Introduction

It is well known that the space radiation environment has a negative impact on the performance of the electronic systems within spacecraft through the damage caused by ionizing and nonionizing radiation. In the case of optoelectronic devices, the decrease in performance is caused by the creation of defects within the silicon bandgap; the impact on the operational performance is then dependent on the defect type, the sensor's operating conditions, and also the sensor type. Lattice defects change the electrical properties of the silicon through a number of different processes, including generation (thermal generation of e-h pairs), recombination (charge is captured and is effectively lost), and trapping (charge is captured and released after some period of time).[1] The impact of these defects is subject to the energy level created within the silicon bandgap, related to the type of impurity forming the defect, the speed at which the charge is moving and the temperature of the silicon. Different detectors are more susceptible to certain types of defects, for example, a charge-coupled device (CCD) requires a number of charge transfers to read out, compared to the one transfer typically required by a complementary metal-oxide semiconductor image sensor (CIS), making the impact of trapping on charge transfer efficiency (CTE) of particular interest to those wishing to use a CCD in space.

A significant amount of work has been performed to minimize the impact of radiation damage on CTE within a CCD, including the use of a p-channel rather than the standard n-channel variant. The increased tolerance to displacement damage of a p-channel CCD was first demonstrated in 1997[2] and since then a number of other studies have demonstrated an improved hardness to radiation-induced charge transfer inefficiency (CTI) when compared to n-channel CCDs.[3–7] The improvement has been linked to the number and type of defects formed within the buried channel, and how these defects impact charge transfer, i.e., how the trap emission time constants relate to the CCD operating speed in both the parallel and serial directions. The defect species, which has the greatest impact on CTI, is the one with a comparable emission time constant to the clock timings, hence why serial and parallel CTI are often different because different clock timings are used. The period of dwell time between transfers (for parallel, this is the time taken to perform the serial readout, and for serial, this is the time taken to perform a parallel transfer into the register) also influences the impact, a defect will have on charge transfer. Optimal charge transfer can be achieved when the emission time constant of traps present within the CCD is significantly faster or significantly slower than the selected clock timings. This is because the trap will likely be released back into the charge packet, described as a "fast trap," or it will remain filled throughout the charge transfer process, described as a "slow trap." Trap pumping can be used to identify these regions of optimal transfer.

The CTI in an n-channel CCD has been shown to increase as a result of the oxygen-vacancy (A-center), an unknown trap at 0.30 eV below the conduction band and the phosphorus-vacancy (E-center). Phosphorous is used to dope the n-type buried channel; it is therefore present in high concentrations and the emission time of the E-center is comparable to the clock periods typically used in CCD operation, thus making it the dominant defect for increasing the CTI. In p-channel CCDs, the dopant used, boron, has not been shown to impact charge transfer giving an inherent reduction in the number of defects formed, which increase CTI when compared to n-channel CCDs. The

*Address all correspondence to: Jason P. D. Gow, E-mail: jason.gow@open.ac.uk

2329-4124/2016/$25.00 © 2016 SPIE

radiation-induced defects, which increase CTI in a p-channel CCD, have been linked to the divacancy and other traps related to carbon and oxygen interstitials.[3–8] As there are less radiation-induced defects in a p-channel CCD, which have been shown to increase CTI, and because they are formed in smaller quantities (the divacancy is a second-order defect and boron defects have not been shown to impact CTE) when compared to an n-channel equivalent, p-channel CCDs are more hard to radiation-induced CTI. A comparison of the n-channel and p-channel CCD204 performance from a previous room temperature irradiation study can be found in Gow et al.[7] Additional work to improve our understanding of radiation-induced defects and their evolution in both n-channel and p-channel CCDs, using trap pumping, and the impact on charge transfer is planned for 2016. This study will include a side-by-side proton irradiation of a p-channel and n-channel CCD204 both held at 153 K.

It is possible through the selection of sensor type, including the material used for charge collection and transfer (n-channel or p-channel), and by performing a radiation damage mitigation study, to select the optimal operating conditions for use in flight. Typically, this has been performed at room temperature; however, based on the evidence from other studies looking into the performance of devices irradiated at cryogenic temperatures,[6,9–17] this may not be sufficient for the latest precision astronomy missions, where the location of even small amounts of charge needs to be accounted for. The aforementioned studies have shown that performing an irradiation at only room temperature can give misleading impressions of both the evolution of dark current, bright defects,[6,9–11,15–17] and CTE.[6,9,12–17] These factors can have a significant impact on the selection of the optimal operating conditions. It is important not to fall into the trap of performing extensive optimization based on the results of a room temperature study when the defects type and quantities that could impact the performance inflight, where the device is operating cryogenically, could be significantly different.

The study described in this paper is being performed as part of a European Space Agency (ESA)-funded investigation into the performance benefits provided through the use of a p-channel rather than an n-channel CCD.[18] The study used seven e2v technology p-channel CCD204 devices fabricated with exactly the same process as standard n-channel CCDs, but with a simple reversal of dopant polarities, the gate dielectric is the same in both cases. The full study includes a complete electro-optical characterization to determine: optimal operational temperature, charge to voltage conversion factor, global and local photoresponse nonuniformity, read-out noise, nonlinearity, image and register full well capacity, dark signal, dark signal nonuniformity, defects in darkness, charge injection uniformity, parallel and serial CTE, point spread function, modulation transfer function, quantum efficiency, and trap identification by pumping. The overall aim of the ESA-funded study was to build upon our understanding of device behavior, the benefits offered through the use of p-channel CCDs, and also to provide inputs to modeling and simulation activities. The full study includes the irradiation of three p-channel CCD204 devices, where two irradiations were performed at room temperature and one with the device held at 153 K throughout the irradiation and for a period of 1 week after the irradiation. This was then followed by testing at 153 K interspaced by the device being held at room temperature for periods of 26 h, 1 week, and 1 month to assess the impact of holding the device at room temperature on its performance postirradiation.

This paper focuses on some of the early results from the cryogenic irradiation performed with the device operating normally at 153 K and the subsequent impact of the device being allowed to room temperature before cooling back to 153 K. The experimental arrangement and technique are described, followed by some of the initial observations of the dark current, bright defects, and trap evolution postirradiation. The impact of a flat-band voltage shift on the full well capacity of the device is also discussed, including a description of edge effects, something not observed during the irradiation of these devices when unbiased. The CTE performance is complicated by the changes in dark current and trap evolution and will be discussed in a future publication.

1.1 *CCD204*

The e2v technologies CCD204, shown in Fig. 1, is manufactured on high-resistivity bulk n-type silicon thinned to 70 μm (fully depleted). It is a 4k × 1k device with 12 μm square pixels, utilizing a split register with two output nodes, each of which can be operated using an amplifier responsivity of 4.5 or 1.5 $\mu V/h^+$. It is based on the same architecture used in the CCD203, previously flown on board the Solar Dynamics Observatory launched in 2010,[18] but with the inclusion of a charge injection structure. Both p-channel[7,19] and n-channel[20] variants have been produced.

The serial register of the CCD204 is designed to allow on-chip pixel-signal binning to be possible, resulting in a channel width of 50 μm. The custom CCD273 developed for the Euclid visible imager[18,21] is based on the CCD204, but as binning is not

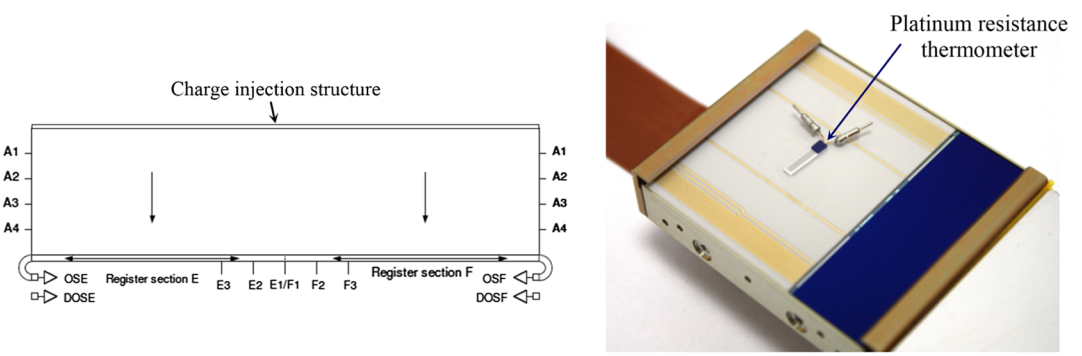

Fig. 1 Schematic and photograph of the e2v technologies CCD204-22. The photograph shows the location of the platinum resistance thermometer used to monitor the temperature of the device during data collection.

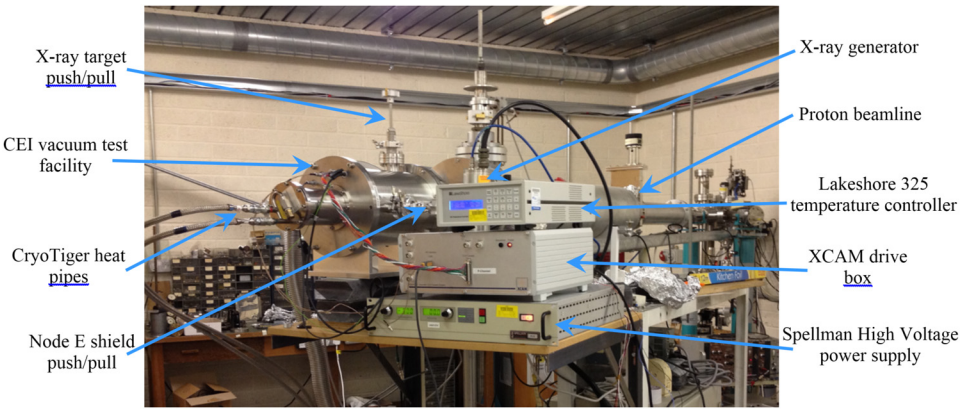

Fig. 2 Photograph of the CEI vacuum chamber attached to the end of the Synergy Health proton beamline.

required, the register width was reduced to 20 μm to provide an improvement in serial CTE. This was measured using Mn-Kα x-rays to give a factor of around 1.7 improvement in serial CTE;[22] the same principle could be applied to the p-channel CCD204 in future variants.

2 Experimental Arrangement

During the irradiation, performed using 7.5-MeV protons from the Synergy Health 5MV Tandem accelerator (United Kingdom), and the data collection, the device under test was held in a modified Centre for Electronic Imaging (CEI) vacuum test facility, as shown in Fig. 2 mounted on the end of the proton beamline. The CCD under test was clamped onto a copper cold bench connected to a CryoTiger® refrigeration system capable of cooling the CCD to around 135 K. The temperature was controlled using a feedback system, comprising a Lakeshore 325 temperature controller, platinum resistance thermometer, and a heater. An XTF5011/75-TH x-ray tube was used to fluoresce a polished manganese target held at 45 deg to the incident x-ray beam to provide around one x-ray event per 80 pixels. Flat field illumination, with the nonuniformity being within 5% across the device, was provided by two light-emitting diodes (LEDs) placed at the far end of the chamber. Clocking and biasing were provided by an XCAM Ltd. USB2REM2 camera drive box in conjunction with the drive software controlled by a custom MATLAB software program.

During the irradiation, the x-ray target was raised out of the beam using the push-pull labeled in Fig. 2. The 10-mm-thick aluminum proton shields, shown in Fig. 3, were attached to rotational push pulls to enable the shields to be moved into, Fig. 3(a), and out of the beam, Fig. 3(b), thereby allowing the two nodes to be irradiated with a different fluence. A shield guide was mounted around the device, indicated in Fig. 3, to ensure that the shields, held 3 mm from the surface of the CCD, could move easily without risk of hitting the surface of the CCD. Rotational push pulls were used both to allow a slight rotation to be applied to hold the shields in place during data collection, shown in Fig. 3(b), but also to allow four different regions to be irradiated for a future application of the test equipment where a larger 4k × 4k CCD273 will be irradiated. The headboard, which contains the preamplifiers for the two output nodes, was also shielded during the irradiation.

During data collection, a gate valve was closed to isolate the test chamber from the beamline; this was included to allow the test chamber to be removed while keeping the device at 153 K and also to isolate it from the beamline, which contains a number of viewing ports. These ports were covered with aluminum foil during the irradiation; however, it is likely that there would still be light leakage making data collection without isolating the chamber unadvisable.

2.1 *Proton Irradiation*

The proton irradiation was performed utilizing three p-channel CCD204s using 7.5-MeV protons from the Synergy Health 5MV Tandem accelerator (United Kingdom). The area irradiated on each device is shown in Fig. 3(a). This region of irradiation was selected to provide an on-chip control, i.e., the region next to the output node was left unirradiated, while

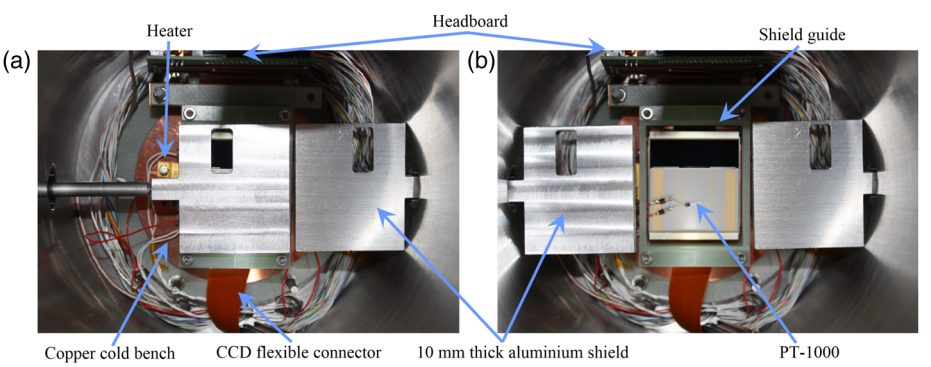

Fig. 3 (a) Aluminum shields in position to irradiate node F and (b) withdrawn for data collection.

Table 1 Proton irradiation details for the room temperature and cryogenic irradiation.

Device	Details	Image region	7.5-MeV proton fluence (protons cm^{-2})	7.5-MeV flux (protons cm^{-2})	10-MeV equivalent proton fluence (protons cm^{-2})
10092–06–02	Control	AE AF		Control device	
10092–04–03	Room temperature	AE	3.07×10^9	2.1×10^7	4.0×10^9
		AF	1.53×10^9	1.8×10^7	2.0×10^9
10092–01–04	Room temperature	AE	7.66×10^{10}	1.5×10^7	1.0×10^{11}
		AF	1.23×10^{10}	1.6×10^7	1.6×10^{10}
10092–04–05	Cryogenic	AE	7.66×10^{10}	3.4×10^7	1.0×10^{11}
		AF	7.65×10^8	3.5×10^7	1.0×10^9

still allowing an assessment of parallel and serial CTE to be performed. Details on the flux and 10-MeV equivalent fluence delivered to each device are given in Table 1.

During the cryogenic irradiation, the CCD was biased and acquiring images, but the majority of the images collected during the irradiation were saturated in signal, with the exception of the lucky image shown in Fig. 4. The start of the image acquisition period occurred after the proton beam had been turned off, so the beam was being powered down as charge was being clocked through the device prior to the start of 10-s integration.

The image clearly shows the area of the device that was unshielded; it also shows a decreasing amount of charged particle interaction outside of the shielded region. Based on previous irradiations, the interaction of protons on the edge of the shielded region was evident by an increased dark current on the edge of the irradiation area, due to protons losing energy within the shield and then causing increased amounts of damage to the detector. It is interesting to note how far across the device protons still interact. It should be noted that the flux in the shielded region will be many orders of magnitude less than the direct irradiation and values recorded in the control region are comparable to preirradiation levels. The irradiated region also indicates a number of charged particle interactions after the beam was powered down; these are the result of material being activated during the irradiation and the subsequent short-lived decay process. The increase in dark current can also be observed and shows the area that received direct irradiation.

3 Experimental Technique

The CCD204 was typically read out at 50 kHz using a parallel transfer pulse time of 1000 μs, but the read-out speed was increased to 100 kHz during the collection of trap pumping data to enable more images to be collected in a reduced period of time. The dark current and number of bright defects were determined using three images taken with an integration time of 324 s. A bright defect was defined as a pixel exhibiting greater than 50 and 200 holes with the surrounding eight pixels being below a threshold of 100 holes; this requirement should be met in three images for the identification of a bright defect to be made. The full well capacity was assessed by reading out the device with the LEDs emitting continuously to provide an increasing amount of charge within the detector as a function of row number, with an additional pause inserted after the

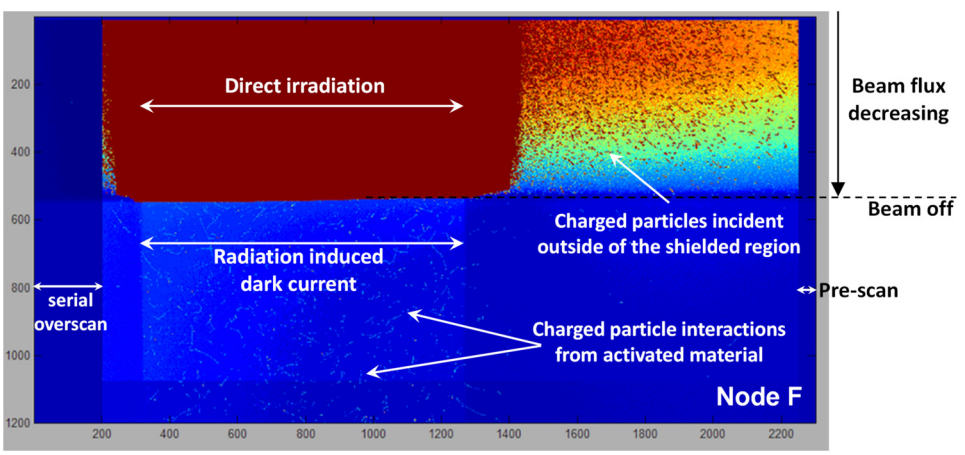

Fig. 4 A lucky image taken as the beam was powered down during the last irradiation. The direct irradiation of the area under the shield, protons scattering within the shield incident in the shielded region, radioactive decays from activated material, and the impact of radiation induced dark current can all be observed.

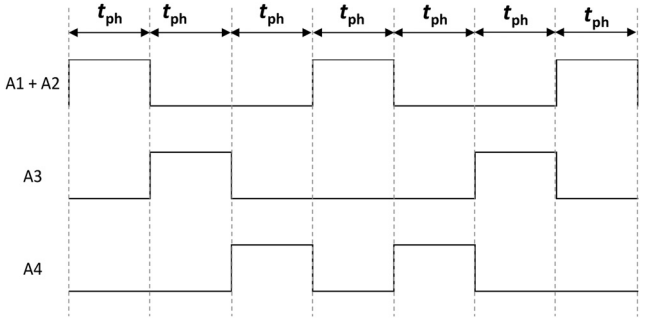

Fig. 5 Clocking scheme used during trap pumping analysis; the phase time, t_{ph}, is varied to identify individual traps emission time constants.

serial line transfer to ensure the full well of the device was exceeded. The full well was defined as the point where the nonlinearity exceeded 3% and referred to as Sat_{Lin}, and is the point at which the potential under the collecting phase is comparable to that of the barrier phase, thereby resulting in charge blooming.

The trap pumping analysis relies on moving the charge backward and forward in the parallel direction using the clocking shown in Fig. 5. The intensity of the resulting dipole is dependent on the phase time, t_{ph}, increasing to the point at which the trap has maximum effect is most efficient and then decreasing as the t_{ph} is increasing further. This is shown in Figs. 6 and 7, which show the dipole intensity as a function of t_{ph} for the divacancy and carbon interstitial defects, respectively. It should be noted that these plots were recorded prior to the irradiation, indicating the presence of both types of defects within the unirradiated silicon. The emission time constant of the trap can then be calculated by fitting

$$\text{Dipole Amplitude} = \text{NP}_\text{C}\left[\exp\left(\frac{-t_{ph}}{\tau_e}\right) - \exp\left(\frac{-2t_{ph}}{\tau_e}\right)\right], \quad (1)$$

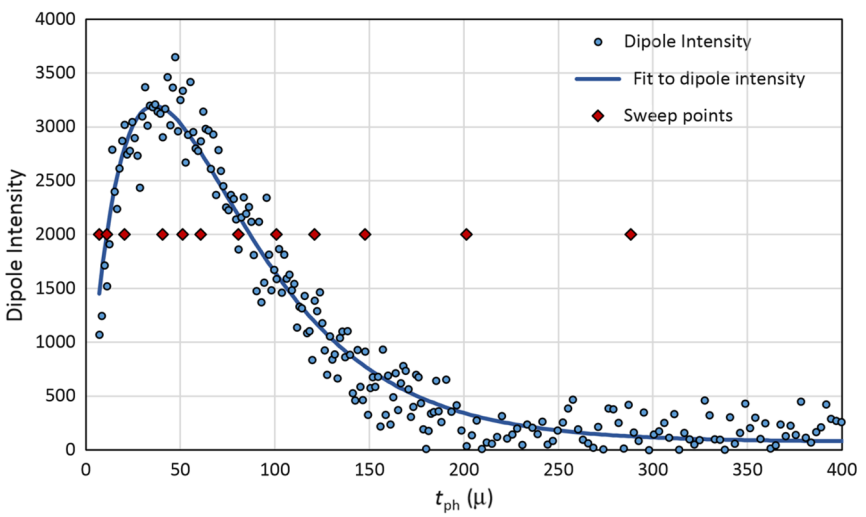

Fig. 6 Dipole intensity as a function of t_{ph} showing a divacancy defect measured preirradiation, the points selected to enable the trap to be quickly identified are indicated by the red circles.

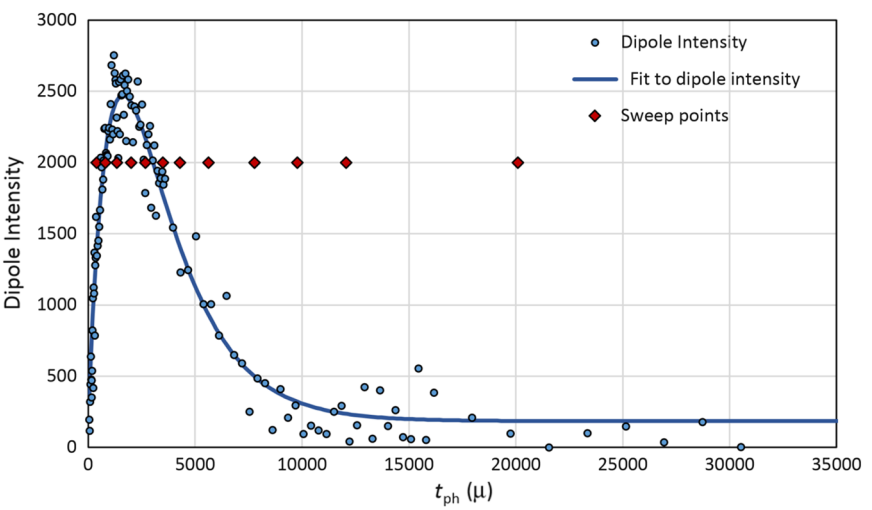

Fig. 7 Dipole intensity as a function of t_{ph} showing a carbon interstitial defect measured preirradiation; the points selected to enable the trap to be quickly identified are indicated by the red circles.

where N is the number of pumping cycles (in this study 4000), P_C is the probability of capture, and τ_e is the emission time constant, to the data in Figs. 6 and 7. The resulting fit to the data is shown in both figures; further information on this method can be found in Hall et al.[23]

This process, depending on the emission time constant of the trap being investigated, requires many hours to provide the number of data points shown in Figs. 6 and 7. To investigate the defect behavior postirradiation, this had to be reduced and two different methods were considered. The first was to operate the device using only a t_{ph} equivalent to the peak amplitude for the two traps that could be investigated, the carbon interstitial and the divacancy. The second was to select key points along the profile and use those to determine the trap type. The issue with the first method is that it relies on the assumption that if a trap is identified using that value of t_{ph}, then it is precisely the trap that is being sought. This could, however, result in erroneous identification should other trap species with similar emission time constants be detected, but it does allow for increased time resolution. The second method increases the accuracy of the identification and allows, to a limited extent when compared to extensive data collection, one to determine subtleties in trap emission time constants while only requiring tens of minutes to complete a full trap sweep. The trap sweeping method was therefore selected for this study. The points used to identify the carbon interstitial and divacancy defects are shown in Figs. 6 and 7, respectively.

4 Results and Discussions

The dark current measured within the device after the irradiation as a function of temperature is shown in Fig. 8; the point at which various irradiations finished and the periods that the device was at room temperature are also indicated. What is evident is that there is a significant increase in dark current after the irradiation, followed by a gradual reduction, which, even after 153 h was still reducing, at a considerable slower rate than immediately after the initial irradiation. After a period at room temperature, there is an 80% decrease in the dark current followed by a continued reduction and, upon being held at room temperature for a further week, the dark current remained within error. The measurement after a further 3 weeks at room temperature was also comparable indicating that the performance has now stabilized to within the error on the measurement. The dark current measured in a device irradiated at room temperature and operated using the same operating conditions is also included in Fig. 8, showing that after the 1-week anneal, the performance is within error of the room temperature measurements. This device was irradiated to a 10-MeV equivalent fluence of 1.0×10^{11} protons cm^{-2}; a linear increase has been used to estimate the dark current at 1.24×10^{11} protons cm^{-2}.

The observed trend in dark current is similar to previously reported behavior,[6] including the second dip after the first period at room temperature. The other irradiated region follows a similar trend. The control regions also exhibit an increase in the dark current recorded; this could be as a result of residual charge left within the serial register after the transfer because the serial register dump function was not used after the completion of each successive read out. Another possibility is that it is the impact of deep traps, which captured charge during the irradiation and are slowly emitting over an extended period of time. It is likely that in-flight operation under continual radiation bombardment will be similar to the performance just prior to the device being brought to room temperature for the first time.

However, it should be noted that although work comparing ground and in-orbit performance has shown similar trends for hot pixels[10] and CTI,[12] the actual values are not the same, which is attributed to device to device behavior and the difference in the incident radiation spectra. To be able to substantiate this claim, comparable data will be required from ground and in-orbit testing. While Euclid is mapping the dark universe, it will also be performing trap pumping, which will be compared to data generated during ground-based cryogenic irradiations. This will provide an excellent opportunity to compare data from a 6-year radiation study in a low-proton flux environment and compare that to the equivalent fluence, which is delivered in minutes. It is also worth noting that Dr. Neil Murray (The Open

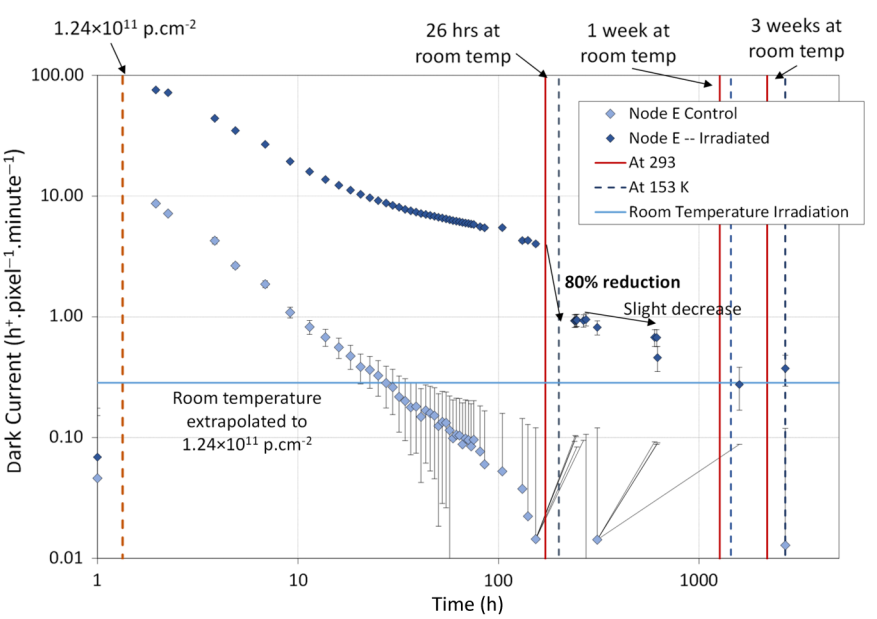

Fig. 8 Dark current as a function of time in the two irradiated regions and their respective control regions. The original 26 h at room temperature and the further time periods are also indicated.

University) has identified pumped charge within the Rosetta navigation camera images,[24] a result of the CCDs using dither mode clocking to minimize surface dark current. This work, once published, should help expand our understanding of the differences between ground testing and the observed performance changes in orbit.

The number of bright defects above 50 and 200 holes (after 324 s) created in node E irradiated with a 10-MeV equivalent proton fluence of 1.24×10^{11} protons cm^{-2} is shown in Fig. 9. As with the dark current, there is a rapid decrease immediately after the irradiation, with values appearing to level out just prior to the device being allowed up to room temperature. After the device was held at room temperature, only one bright defect could be identified using the same criteria. Only a few bright defects were created in node F. Subject to the generation rate and instrument integration time, the formation of bright defects will reduce the effective image area and with a high enough number be problematic for star trackers. A room temperature irradiation could lead to this number being underestimated, whereas a cryogenic irradiation will provide a better understanding and also indicate the benefit of annealing to reduce their number.

The image taken to determine the change in full well capacity using node E irradiated with a 10-MeV equivalent proton fluence of 1.24×10^{11} protons cm^{-2} is shown in Fig. 10. The onset of blooming occurs around 300 rows earlier than in the control region and indicates a decrease in the Sat_{Lin} of around 50,000 holes. The reduction in full well is likely to be the resulting

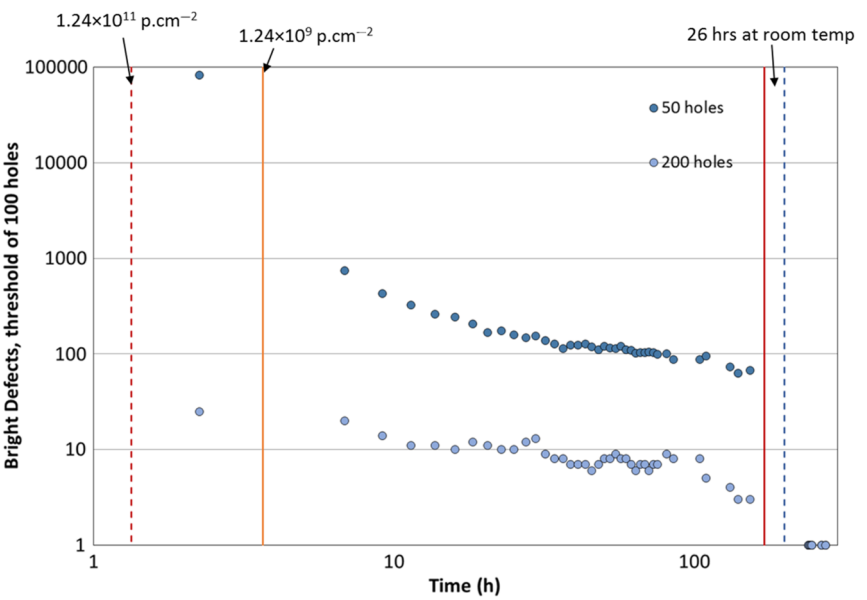

Fig. 9 Number of bright defects as a function of time in the region irradiated with a 10-MeV equivalent proton fluence of 1.24×10^{11} protons cm^{-2}.

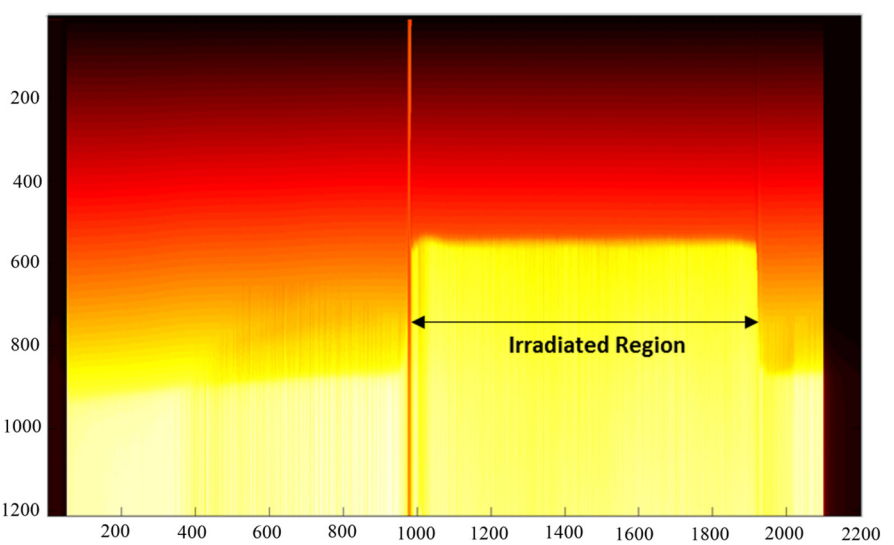

Fig. 10 Image resulting from an LED being powered on while the device is read out. The reduction in full well capacity in the region irradiated with a 10-MeV equivalent fluence of 1.24×10^{11} protons cm^{-2} is evident by the step change increase in signal as the device becomes saturated in that region.

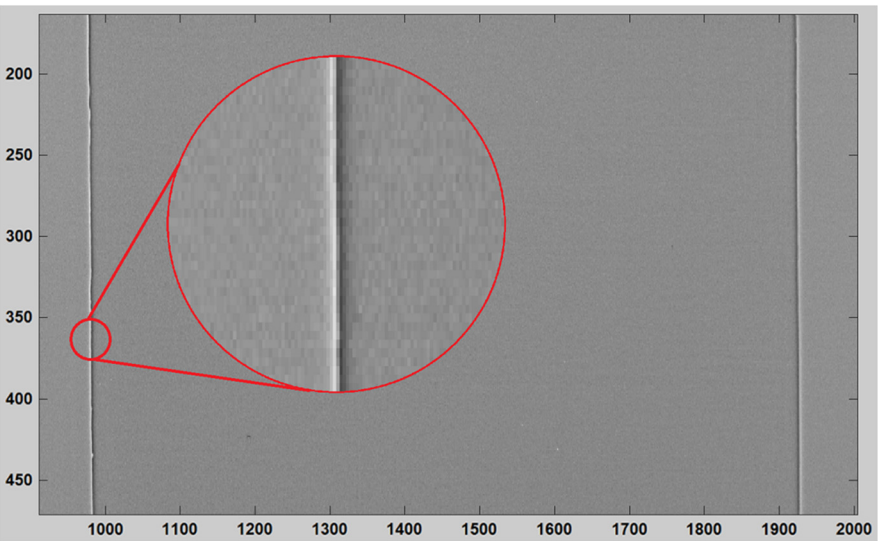

Fig. 11 Image taken using a flat field exposure of 20,000 holes, cropped to show the area irradiated with a 10-MeV equivalent fluence of 1.24×10^{11} protons cm^{-2} and the charge redistribution, which occurs on the boundaries of the irradiation.

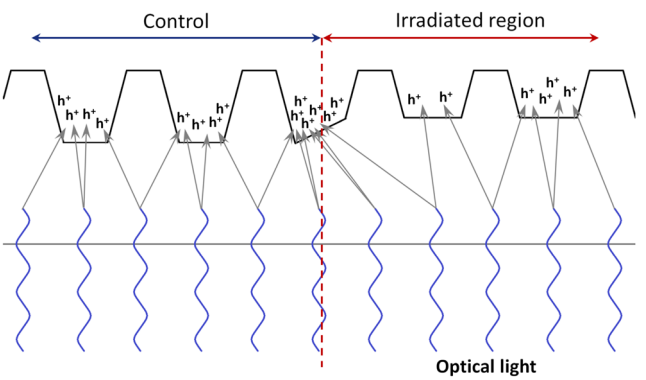

Fig. 12 Simplification of the process, which occurs at the edges of the irradiation, where charge preferentially moves toward regions with the greatest potential.

flatband voltage, which occurs during the irradiation, in e2v n-channel CCDs, this is typically 100 to 200 mV/krad for a standard gate CCD (for example, the p-channel and n-channel CCD204).[25] The total ionizing dose (TID) delivered during the irradiation was 65 krad. Assuming the voltage shift is linear and using preirradiation data from device 10092-04-03, where the full well was measured as a function of clock voltage, the initial estimate of the flatband voltage shift was found to be around 30 mV/krad. This is with the same gate dielectric and thickness, as stated in Sec. 1 and, consequently, the reason for the significantly smaller shift is difficult to explain. Our original interpretation[26] of the cause was due to the formation of trapped holes in the oxide being compensated by electrons trapped in the Si_3N_4 (of the Si_3N_4-SiO_2 gate dielectric), thereby resulting in a lower flatband shift described by Saks et al.[27] However, this

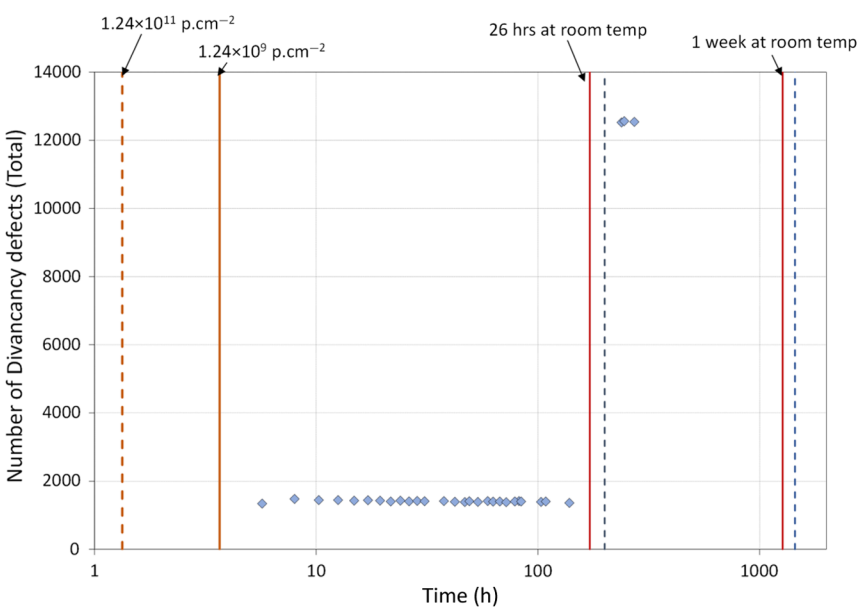

Fig. 13 Number of divacancy defects recorded after the irradiation as a function of time.

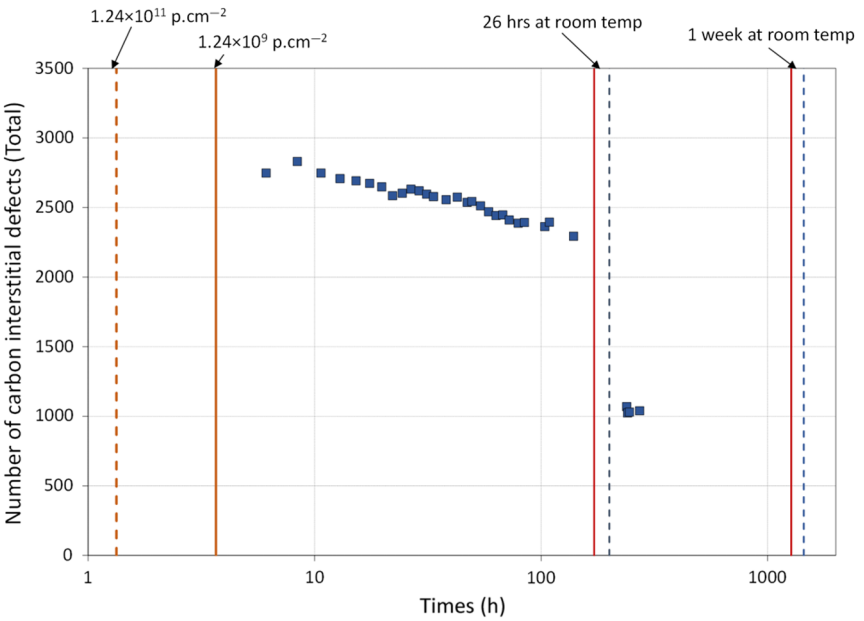

Fig. 14 Number of carbon interstitial defects recorded after the irradiation as a function of time.

original interpretation was incorrect because e2v n-channel CCDs also benefit from this process.[25]

The other interesting phenomena that can be observed in Fig. 10 are the two bands, which mark the edge of the irradiated region of the device; a close-up image is shown in Fig. 11 taken using a uniform flat field exposure of 20,000 holes. The edge effects are perfectly aligned with the region of increased dark current. The same effect cannot be observed in node F and the bands are not observed in a device, which was irradiated at room temperature and unbiased to a comparable proton fluence. The cause of this effect is likely to do with the preferential movement of charge toward a region of increased potential resulting in the redistribution of charge and the formation of light and dark bands at the edge of the irradiated region; a cartoon of the process is shown in Fig. 12. The process is the same as that which occurs during point-spread function measurements commonly referred to as the brighter-fatter effect;[28] however, in this case, the description of charge redistribution[29] is more appropriate.

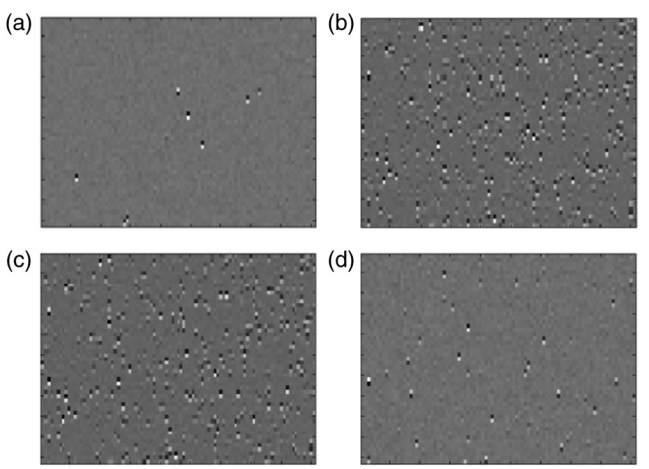

Fig. 15 Image showing the results of trap pumping in a section of the (a) device preirradiation, (b) 6 min after the irradiation was complete, (c) 18 min after the irradiation was complete and (d) a difference image showing the change over a period of 12 min.

The number of defects identified in a region of 239,000 pixels as a function of time after the irradiation is shown in Fig. 13 for the divacancy and Fig. 14 for the carbon interstitial. In both cases, there is an increase in the number of defects after the irradiation, followed by a gradual reduction as the device remained at 153 K. Data were collected closer to the end of the irradiation using the trap sweeping method. However, the presence of charged particle interaction requires more in-depth analysis to ensure the correct number of traps can be determined. The increase in the number of traps after the irradiation was confirmed by looking at trap-pumping images taken as soon as the kit could be accessed after the irradiation was complete, as shown in Fig. 15. The number of traps in the same region of the device is shown prior to the irradiation, Fig. 15(a), 6 min after the irradiation, Fig. 15(b), and 18 min after, Fig. 15(c), with a differenced image, Fig. 15(d), showing the increase in number of traps over the period of 12 min. After the device was held at room temperature, the number of divacancy defects has increased by around a factor of 9. It should be noted that although the divacancy is not mobile at this temperature, the vacancy is mobile. The number of carbon interstitial defects has decreased by around 50% after 26 h at room temperature. The carbon interstitial is mobile at room temperature and is therefore able to form other stable defects. A more detailed analysis of the data is currently underway, looking at the behavior of individual traps and the impact on their emission time constants after the period at room temperature; this will form part of a future publication once the analysis has been completed.

5 Conclusions

The behavior of a number of parameters is highly dynamic immediately postirradiation. Monitoring everything is challenging, and it could be advisable in a future irradiation to focus primarily on one parameter with occasional monitoring of other parameters. Both the dark current and the number of bright defects exhibit a rapid decline postirradiation and even after

150 h have not yet stabilized. It is likely that in-flight performance would be similar to the performance at which stabilization occurs. However, before this can be confirmed, it would be advisable to perform irradiations at different flux rates and monitor the performance until the parameters of interest have stabilized.

Although the nature of p-channel silicon means that the full well capacity of the device is reduced with incident ionizing radiation, it has been shown that the flatband voltage shift, calculated to be 30 mV/krad, is significantly less than in a standard gate n-channel CCD. This makes p-channel devices suitable for use in high TID environments. This will be investigated further by irradiating an n-channel and p-channel CCD204 side by side during a gamma irradiation. The identification of preferential charge redistribution is also of interest; although in normal operation, it is unlikely that such a step change in dose across the device would be incurred so as to make it an issue for inflight operation.

The evolution of the two defects explored through the use of trap sweeping is extremely interesting and provides a window into the behavior of individual defects as they are both formed and anneal over periods of time, both with the device held at 153 K and also after a period of time spent at room temperature. The order of magnitude increase in the number of divacancy defects after the first room temperature anneal is significant because this defect has an emission time constant, which is similar to the serial transfer timings, indicating improved serial charge transfer when held at cryogenic temperature. A significant quantity of data has been collected to allow a more detailed investigation into this behavior to be performed and will form party of a future publication.

The impact on the CTE of both the changing dark current and number of trapping defects makes the analysis of CTE more complicated than previous radiation campaigns where data collection was performed under stable operating conditions, i.e., fixed dark current and trap numbers. Therefore, further analysis of the CTE is required and will be described in a future publication.

Data continue to be collected with the cryogenically irradiated device after increasing periods at room temperature and the data collection and analysis of the room temperature irradiated devices will also be completed in the near future, allowing a comparison of the two datasets and with previously irradiated n-channel CCDs to be performed. It would also be advisable to continue to monitor the device performance over an extended period of time, i.e., years, to identify possible continued changes in performance. The equipment and methodologies developed as part of this study have already been utilized in an n-channel cryogenic irradiation study that is currently ongoing. The equipment will also be used, and slightly modified, for a planned future n-channel CCD irradiation, which will include a "keep cold and return" irradiation, where the device will be transported back to the CEI for monitoring over an extended period of time (years) to allow comparison to data collected onboard the ESA Euclid spacecraft while in orbit.

It is likely that with the continued development of precision astronomy missions, performing an optimization of the operating speeds and temperature after the device has been irradiated cryogenically will be highly recommended. This will ensure the most efficient timings can be selected and avoid optimizing for a trap species, which will actually have negligible impact (trap density increases after time at room temperature) or select comparable timings for a trap, which had could anneal at room temperature (trap density decreases after time at room temperature) and would actually have a significant impact on CTI when operating under mission appropriate conditions (i.e., staying cold). The temperature aspect requires a study to confirm if the same performance is achieved if the device is irradiated at one temperature to if it is irradiated colder and then allowed to warm to that temperature. This is planned for the near future and will include the side-by-side irradiation of an n-channel and p-channel CCD204.

Acknowledgments

The authors would like to thank Keith Jones of Synergy Health for his assistance during the proton irradiation, and Ludovic Duvet, Thibaut Prodhomme and Alessandra Ciapponi of ESA for their support during this study.

References

1. J. R. Srour, C. J. Marshall, and P. W. Marshall, "Review of displacement damage effects in silicon devices," *IEEE Trans. Nucl. Sci.* **50**(3), 653–670 (2003).
2. J. P. Spratt, B. C. Passenheim, and R. E. Leadon, "The effects of nuclear radiation on P-channel CCD imagers," in *IEEE Radiation Effects Data Workshop*, pp. 116–121, IEEE, Snowmass Village, Colorado (1997).
3. G. R. Hopkinson, "Proton damage effect on P-channel CCDs," *IEEE Trans. Nucl. Sci.* **46**(6), 1790–1796 (1999).
4. C. Bebek et al., "Proton radiation damage in P-channel CCDs fabricated on high-resistivity silicon," *IEEE Trans. Nucl. Sci.* **49**(3), 1221–1225 (2002).
5. J. P. Spratt et al., "Proton damage effects in high performance P-channel CCDs," *IEEE Trans. Nucl. Sci.* **52**(6), 2695–2702 (2005).
6. K. Dawson et al., "Radiation tolerance of fully-depleted P-channel CCDs designed for the SNAP satellite," *IEEE Trans. Nucl. Sci.* **55**(3), 1725–1735 (2008).
7. J. P. D. Gow et al., "Proton damage comparison of an e2v technologies n-channel and p-channel CCD204," *IEEE Trans. Nucl. Sci.* **61**(4), 1843–1848 (2014).
8. N. J. Mostek et al., "Charge trap identification for proton-irradiated p+ channel CCDs," *Proc. SPIE* **7742**, 774216 (2010).
9. R. A. Kimble, P. Goudfrootij, and R. L. Gilliland, "Radiation damage effects on the CCD detector of the space telescope imaging spectrometer," *Proc. SPIE* **4013**, 532 (2000).
10. E. J. Polidan et al., "Hot pixel behavior in WFC3 CCD detectors irradiated under operational conditions," *Proc. SPIE* **5167**, 258 (2004).
11. C. J. Marshall et al., "Hot pixel annealing behavior in CCDs irradiated at -84 °C," *IEEE Trans. Nucl. Sci.* **52**(6), 2672–2677 (2005).
12. M. Bautz et al., "Anomalous annealing of a high-resistivity CCD irradiated at low temperature," *IEEE Trans. Nucl. Sci.* **52**(2), 519–526 (2005).
13. C. E. Grant et al., "Physics of reverse annealing in high-resistivity Chandra ACIS CCDs," *Proc. SPIE* **7021**, 702119 (2008).
14. G. Hopkinson et al., "Radiation effects on astrometric CCDs at low operating temperatures," *IEEE Trans. Nucl. Sci.* **52**(6), 2664–2671 (2005).
15. G. Hopkinson and A. Mohammadzadeh, "CCD radiation testing at low temperatures using a laboratory alpha particle source," *IEEE Trans. Nucl. Sci.* **53**(6), 3758–3763 (2006).
16. G. Hopkinson, P. Gare, and G. Sarri, "Effects of low temperature proton irradiation on a large area CCD for astrometric applications," *IEEE Trans. Nucl. Sci.* **57**(4), 2035–2043 (2010).
17. J. P. D. Gow et al., "Proton irradiation of a CCD236 swept charge device at cryogenic temperature and the subsequent annealing," *J. Instrum.* **10**, C01037 (2015).
18. J. Endicott et al., "Charge-coupled devices for the ESA Euclid M-class mission," *Proc. SPIE* **8453**, 845304 (2012).
19. N. J. Murray et al., "Assessment of the performance and radiation damage effects under cryogenic temperatures of a P-channel CCD204s," *Proc. SPIE* **9154**, 91540P (2014).

20. J. P. D. Gow et al., "Assessment of space proton radiation-induced charge transfer inefficiency in the CCD204 for the Euclid space observatory," *J. Instrum.* **7**, C01030 (2012).
21. M. Cropper et al., "VIS: the visible imager for Euclid," *Proc. SPIE* **9143**, 91430J (2014).
22. J. P. D. Gow et al., "Assessment of proton radiation-induced charge transfer inefficiency in the CCD273 detector for the Euclid dark energy mission," *Proc. SPIE* **8453**, 845316 (2012).
23. D. J. Hall et al., "Determination of in situ trap properties in CCDs using a single-trap pumping technique," *IEEE Trans. Nucl. Sci.* **61**(4), 1826–1833 (2014).
24. N. J. Murray, "Measured space radiation damage from artefacts in Comet 67P images, presented to the Royal Photographic Society, Imperial College," (2015).
25. D. Burt et al., "Improving radiation tolerance in e2v CCD sensors," *Proc. SPIE* **7439**, 743902 (2009).
26. J. P. D. Gow et al., "Initial results from a cryogenic proton irradiation of a p-channel CCD," *Proc. SPIE* **9601**, 96010F (2015).
27. N. S. Saks et al., "A radiation hard MNOS CCD for low temperature applications," *IEEE Trans. Nucl. Sci.* **26**(6), 5074–5079 (1979).
28. P. Antilogus et al., "The brighter-fatter effect and pixel correlations in CCD sensors," *J. Instrum.* **9**, C03048 (2014).
29. A. Edgar et al., "Point-spread function and photon transfer of a CCD for space-based astronomy," *Proc. SPIE* **8860**, 88600I (2013).

Jason P. D. Gow is a research fellow in the Centre for Electronic Imaging at the Open University UK and was awarded his PhD from Brunel University for work on radiation damage mitigation for the detectors used in the C1XS instrument. He is interested in predicting, understanding, and mitigating the impact of radiation damage on CCD and CMOS detectors for space applications, through environmental modeling and the experimental analysis of device performance.

Daniel Wood is a PhD student at the Centre for Electronic Imaging at the Open University, United Kingdom. His work focuses on the study of radiation damage effects in both n- and p-channel silicon CCDs, specifically regarding lattice damage effects. Prior to joining the group, he completed an MPhys with particle physics and cosmology at the University of Lancaster.

Neil J. Murray is a research fellow at the Centre for Electronic Imaging at the Open University, United Kingdom, and was awarded his PhD from Brunel University for work on improvements to MOS CCD technology for future x-ray astronomy missions. His current research interests include understanding of trap effects and device design/manufacture on charge transfer efficiency, charge redistribution and blooming effects in thin-gate deep-depleted CCDs. He is the principal investigator on the ESA-funded p-channel study.

David Burt works for e2v technologies and is a world expert with a wealth of experience in the design and manufacture of semiconductor devices. He has worked at GEC Hirst Research Labs and e2v throughout the history of CCDs, and has introduced many innovative changes to CCD design for improved performance.

David J. Hall is a research fellow in the Centre for Electronic Imaging at the Open University, United Kingdom. He studied physics at the University of Oxford before completing his PhD at the Open University, researching the impact of detection physics in x-ray CCD imagers and spectrometers. During the last 9 years, he has specialized in radiation damage in detectors and radiation-induced defects in silicon, working on many ESA missions, including Gaia and Euclid.

Ben Dryer is a project officer in the Centre for Electronic Imaging at the Open University, United Kingdom. He completed his PhD at the Open University in 2013 for the study of radiation damage and x-ray spectroscopic performance in CMOS active pixel sensors (APSs) and is interested in how the technology can be improved to compete with CCDs for space applications, for both astronomy and planetary observation.

Andrew D. Holland is a professor in electro-optics and head of the Centre for Electronic Imaging at the Open University, United Kingdom. He is an expert in detector physics and has worked on the development of a number of successful space instruments. Working on a range of detector developments over the past two decades, he has a wealth of knowledge and experience advising on instrument related issues, in particular, radiation damage effects.